Nanoscale Res Lett (2006) 1:20–31
DOI 10.1007/s11671-006-9009-5

NANO REVIEW

Self-assembled GaInNAs/GaAsN quantum dot lasers: solid source molecular beam epitaxy growth and high-temperature operation

S. F. Yoon · C. Y. Liu · Z. Z. Sun · K. C. Yew

Published online: 26 July 2006

Abstract Self-assembled GaInNAs quantum dots (QDs) were grown on GaAs (001) substrate using solid-source molecular-beam epitaxy (SSMBE) equipped with a radio-frequency nitrogen plasma source. The GaInNAs QD growth characteristics were extensively investigated using atomic-force microscopy (AFM), photoluminescence (PL), and transmission electron microscopy (TEM) measurements. Self-assembled GaInNAs/GaAsN single layer QD lasers grown using SSMBE have been fabricated and characterized. The laser worked under continuous wave (CW) operation at room temperature (RT) with emission wavelength of 1175.86 nm. Temperature-dependent measurements have been carried out on the GaInNAs QD lasers. The lowest obtained threshold current density in this work is ~1.05 kA/cm^2 from a GaInNAs QD laser ($50 \times 1{,}700$ μm^2) at 10 °C. High-temperature operation up to 65 °C was demonstrated from an unbonded GaInNAs QD laser ($50 \times 1{,}060$ μm^2), with high characteristic temperature of 79.4 K in the temperature range of 10–60 °C.

Keywords GaInNAs · Quantum dot · Laser diodes · Molecular beam epitaxy (MBE)

S. F. Yoon (✉) · C. Y. Liu · Z. Z. Sun · K. C. Yew
Compound Semiconductor and Quantum Information Group School of Electrical and Electronic Engineering, Nanyang Technological University, Nanyang Avenue, Singapore 639798, Rep. of Singapore
e-mail: esfyoon@ntu.edu.sg

Introduction

Long-wavelength 1.3 μm or 1.55 μm semiconductor lasers are key devices for optical fiber communications and have attracted much attention in recent years due to their zero dispersion and minimal absorption in silica fibers. Nowadays, nearly all commercialized semiconductor lasers operating at wavelength of 1.3 μm and 1.55 μm are made from the InGaAsP/InP material system. The InGaAsP/InP material system, however, exhibits relatively poor electron confinement in the well layers due to rather small band offsets in the conduction band between the well and cladding layers ($\Delta E_c = 0.4\ \Delta E_g$). As a result, such lasers demonstrate relatively inferior high temperature characteristics, namely, device performance is strongly temperature dependent [1]. Although the lasing properties of 1.3-μm and 1.55-μm InGaAsP/InP lasers have been improved using strained multi-quantum well (QW) layers, the performance at high temperature is still unsatisfactory compared with that of short-wavelength lasers on GaAs substrate [2].

Therefore, there has been a large research effort to find GaAs-based solutions to realize 1.3 μm and 1.55 μm lasers. GaInNAs is a promising candidate for long wavelength emission first proposed by Kondow et al. [3, 4]. For many years it was believed that there was no suitable alloy lattice-matched to GaAs at emission wavelength > 1.1 μm. Contrary to the general rules of III–V alloy semiconductors, where a smaller lattice constant increases the bandgap, the large electronegativity of N and its small atomic size results in strong negative bowing parameter. The addition of N to GaAs or InGaAs significantly decreases the bandgap and lattice constants. Adding In

reduces the bandgap, while increasing the lattice constant. By combining N and In, a rapid decrease in bandgap in GaInNAs is obtained; thus allowing the possibility to reach long wavelength emission with simultaneous control over the bandgap and lattice matching to GaAs [3–6]. Figure 1 shows the relationship between the lattice constant and bandgap energy in III–V alloy semiconductors, taking into account the significant bandgap bowing in GaAsN [4]. It can be seen that the N-containing III–V semiconductors significantly expand the application area of III–V alloy semiconductor and increase the freedom for designing semiconductor devices [3, 4]. Since GaInNAs is grown on GaAs substrate, the technically matured GaAs/AlGaAs distributed Bragg reflectors (DBRs) can be used in the GaInNAs vertical cavity surface emitting lasers (VCSELs). The GaAs/AlGaAs bi-layer has larger index difference (~0.7) than the InGaAsP/InP combination. This allows for easier fabrication of DBRs for GaInNAs/GaAs-based devices. Furthermore, GaInNAs/GaAs QW exhibits a large conduction band offset, thus allowing for better thermal performance in GaAs-based GaInNAs lasers. These remarkable fundamental properties of Ga(In)NAs alloys provide an opportunity to tailor the material properties for desired applications in optoelectronic devices based on III–V materials [3–6].

Due to above advantages, in the past few years, there has been considerable interest in GaInNAs materials grown on GaAs substrate for realizing low-cost, high-performance and high-temperature laser diodes in the 1.3 μm and 1.55 μm wavelength region. So far, GaInNAs QW laser performance has been improved significantly [3–19]. Both GaInNAs Fabry-Perot edge-emitting lasers [3–18] and VCSELs [19] have been realized. For edge-emitting 1.3-μm GaInNAs lasers, Tansu et al. [14] reported the lowest

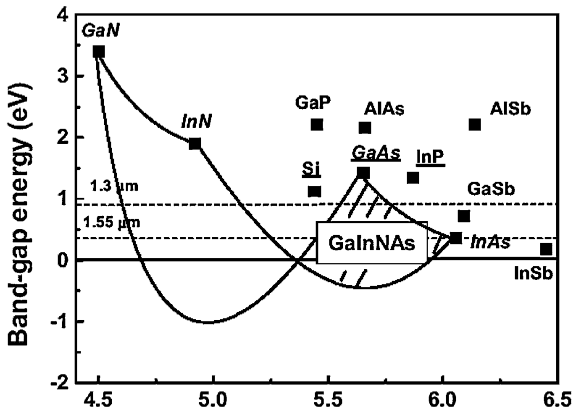

Fig. 1 The relationship between the lattice constant and bandgap energy in III–V alloy semiconductors [4]

transparency current density (J_{tr}) of 75–80 A/cm^2 from structures grown by metal organic chemical vapor deposition (MOCVD); Wang et al. [11] recently reported J_{tr} of 84 A/cm^2 from 1.3-μm GaInNAs lasers, grown using molecular beam epitaxy (MBE). More recently, 10-Gb/s transmission using floor free GaInNAs triple-QW (TQW) ridge waveguide (RWG) lasers have been successfully demonstrated [13]. Undoubtedly, GaInNAs 1.3-μm QW lasers present excellent potential for telecommunication application.

Meanwhile, studies on GaInNAs quantum dot (QD) structures have also attracted much interest, since QD lasers, with three-dimensional carrier confinement, are anticipated to have many advantages over their QW counterparts, such as decreased J_{tr}, increased differential gain, high characteristic temperature (T_0), and largely extended emission wavelength [20, 21]. Moreover, in the case of GaInNAs QD lasers, reduction in bandgap energy with N incorporation decreases the dot sizes for long wavelength emission. Smaller dots have larger subband energy difference, resulting in suppression of carrier leakage to high energy states. Furthermore, smaller dot sizes are also advantageous for obtaining high QD density [22]. Compared to GaInNAs QW, the advantage of using GaInNAs QDs is the expectation to achieve the same long wavelength emission with relatively lower N content; an effect assisted by the wavelength extension ability of the strained 3D islands. The high N content needed for long wavelength emission in GaInNAs QW lasers deteriorates the optical characteristics of the material and limits the device performance. It is hoped that the lower N content in GaInNAs QDs will help alleviate this problem without compromising device performance.

Recently, GaInNAs QDs have been successfully grown using MBE [23–30], chemical beam epitaxy (CBE)[22, 31–34] and MOCVD [35–38]. Photoluminescence (PL) emission in the 1.3 μm and 1.5 μm region from MBE-grown GaInNAs QDs has been observed [23]. However, compared with a large amount of research on GaInNAs QW lasers [3–19], relatively fewer results on GaInNAs QD lasers have been reported [30, 31, 38]. Makino et al. first reported pulsed lasing from a CBE-grown $Ga_{0.5}In_{0.5}N_{0.01}As_{0.99}$ QD laser at 77 K at emission wavelength of 1.02 μm and threshold current density (J_{th}) of 1.9 kA/cm^2 [31]. Recently, Gao et al. reported pulsed lasing from MOCVD-grown GaInNAs QD RWG lasers at room temperature (RT) with emission wavelength at 1078 nm [38]. However, their GaInNAs QD RWG laser (4 × 800 μm^2) showed relatively high J_{th} of ~13 kA/cm^2. We have recently achieved RT continuous wave (CW) operation of $Ga_{0.7}In_{0.3}N_{0.01}As_{0.99}$ QD edge-emitting lasers, grown by

solid source MBE (SSMBE). To the best of our knowledge, this is the first ever report on RT, CW lasing from GaInNAs QD lasers [30].

This paper deals with the various aspects of material characteristics of self-assembled GaInNAs QD structure grown by SSMBE using a radio-frequency nitrogen plasma source. Structural and optical properties of GaInNAs QD structures have been extensively investigated using atomic force microscopy (AFM), PL, and transmission electron microscopy (TEM) measurements. The effect of growth temperature and intermediate layer on GaInNAs QD properties is discussed. GaInNAs/GaAsN single layer QD lasers have been fabricated and characterized. The laser worked under RT, CW operation with emission wavelength centered at 1175.86 nm. Temperature-dependent measurements have also been carried out on the GaInNAs QD lasers of various cavity lengths. The lowest obtained J_{th} in this work is ~1.05 kA/cm^2 from a GaInNAs QD laser ($50 \times 1{,}700$ μm^2) at 10 °C. High-temperature operation up to 65 °C was successfully demonstrated from an unbonded GaInNAs QD laser ($50 \times 1{,}060$ μm^2), with high T_0 of 79.4 K in the temperature range of 10–60 °C.

Experimental details

The GaInNAs QD structures were grown on GaAs (100) by SSMBE with plasma assisted N source. The N composition in the GaInNAs QDs and GaAsN barriers was kept at 1% by controlling the flow rate of high purity nitrogen and rf power, while the In composition was varied from 30% to 100% for different samples. The GaInNAs QD layers were grown at 480–500 °C under As_4/Ga beam equivalent pressure ratio of 18. During GaInNAs deposition, the reflection high-energy electron diffraction (RHEED) pattern transformed from streaky to spotty characteristic, indicating initiation of the self-organized islanding process of two-to-three dimensional transition. AFM measurements were performed in uncapped GaInNAs QD samples grown under identical conditions. PL measurements were performed in a closed-cycle helium cryostat. The PL spectrum was excited by an Ar^+ 514.5 nm laser and detected by a cooled Ge detector. The formation of GaInNAs QDs was extensively confirmed to follow the conventional Stranski-Krastanow (SK) growth mode. Furthermore, AFM observation of change in surface morphology of samples with different GaInNAs monolayer (ML) thickness confirms the nucleation of QDs after a certain number of MLs. The existence of GaInNAs dots in capped samples was also observed by TEM. With AFM, PL, and TEM measurements, structural and optical properties of GaInNAs QD structures have been extensively investigated. Furthermore, the effects of growth temperature and intermediate layer on GaInNAs QD properties were also studied.

For the GaInNAs QD laser studied here, the QD active region consisted of a 28-ML $Ga_{0.7}In_{0.3}N_{0.01}As_{0.99}$ QD layer with two 5-nm-thick $GaAsN_{0.01}$ barrier layers, which was inserted between the undoped 0.1-μm-thick GaAs waveguide layers. The whole waveguide core was then inserted between the 1.5-μm-thick n- and p-type $Al_{0.35}Ga_{0.65}As$ cladding layers. Finally, a 200-nm-thick p^+-GaAs cap layer was grown for electrical contact purpose. Carbon and silicon were used as the p- and n-type dopants, respectively.

Self-assembled GaInNAs QD broad area lasers were fabricated with contact stripe width (w) of 50 μm using conventional SiO_2 confinement method. P-type ohmic contact layers (Ti/Au, 50/250 nm) were deposited by electron beam evaporation. The wafer substrates were then lapped down to about 100 μm thick to facilitate laser chip cleaving. AuGe alloy (Au 88% by weight, 150 nm) and Ni/Au multiple layers (30/250 nm) were deposited by electron beam evaporation on the thinned and polished n-GaAs substrate as n-type ohmic contact. The wafers were then annealed at 410 °C for 3 min in N_2 ambient to alloy both the p-type and n-type ohmic contacts. After fabrication, individual GaInNAs QD lasers were then cleaved at different cavity length (L) for measurement of laser output power (P) versus injection current (I) ($P - I$) characteristics without facet coating. The devices were tested under both CW and pulsed operation. For the CW testing, the GaInNAs QD lasers were p-side-down bonded onto copper heat sinks. Temperature-dependent $P - I$ characteristics have also been tested on the as-cleaved, unbonded GaInNAs QD lasers. In order to reduce the device heating, the temperature-dependent measurements were carried out under pulsed operation at pulse frequency of 20 kHz, pulse width of 500 ns, and duty cycle of 1%. The temperature of the laser was controlled by a thermoelectrically cooled circuit (TEC), which can be varied from 10 °C to 80 °C. The output power of the laser (from one facet) was measured by a calibrated InGaAs photodetector mounted in an integration sphere.

Results and discussion

Figure 2(a–c) shows the AFM images of the surface morphology of $Ga_{0.6}In_{0.4}N_{0.01}As_{0.99}$ QD samples of different thickness from 3 ml to 6 ml grown by SSMBE

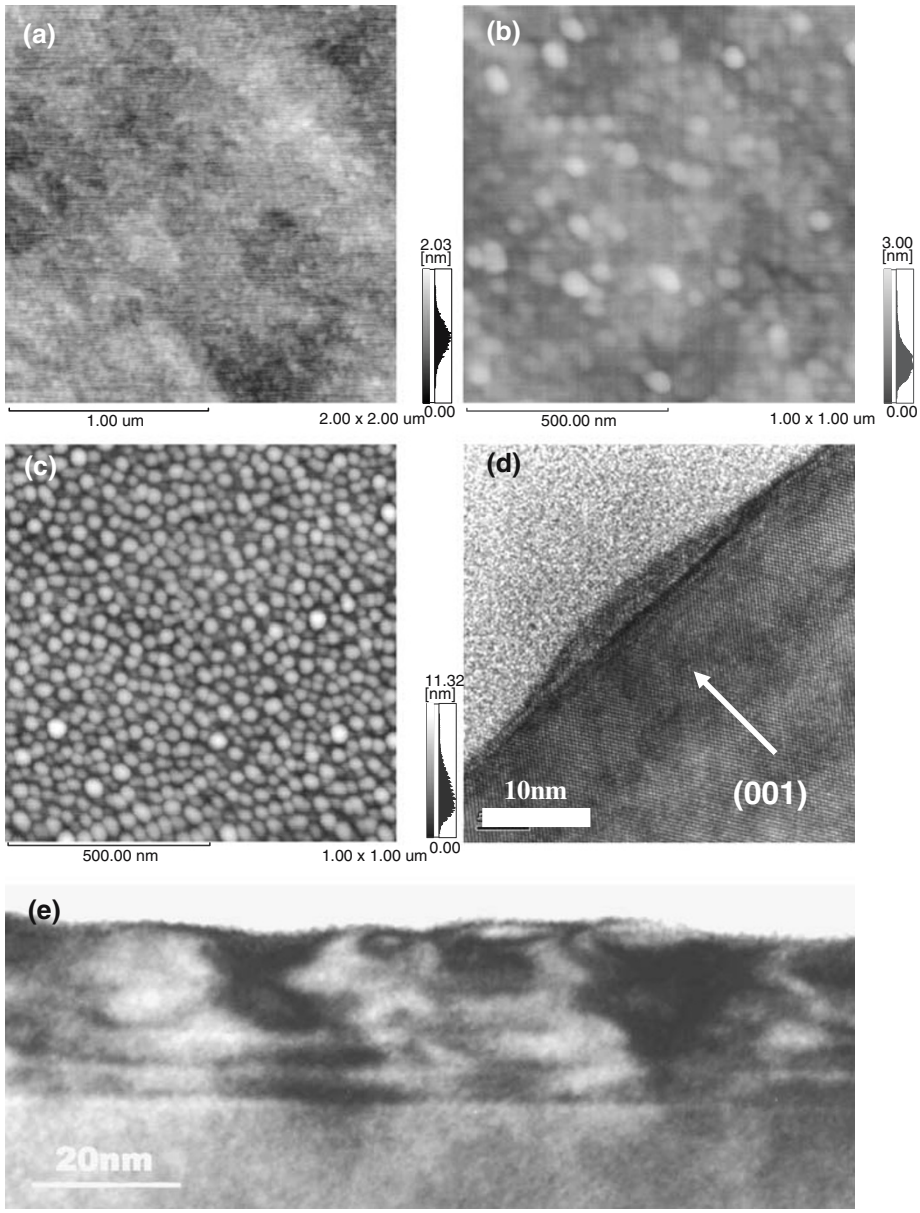

Fig. 2 AFM images of: (**a**) 3 ml-thick, (**b**) 4 ml-thick, and (**c**) 6 ml-thick $Ga_{0.6}In_{0.4}N_{0.01}As_{0.99}$ QD samples. Cross-sectional TEM images of (**d**) 4.5 ml-thick $Ga_{0.6}In_{0.4}N_{0.01}As_{0.99}$ QDs and (**e**) 5 ml-thick $Ga_{0.5}In_{0.5}N_{0.01}As_{0.99}$ QDs multilayer

at 0.5 ml/s and As_4/Ga beam equivalent pressure (BEP) ratio of 18. As shown in Fig. 2a, the surface appears to be atomically flat at 3 ml thickness, with root mean square (RMS) roughness of ~0.4 nm. When the GaInNAs thickness is increased to 4 ml, low density (~1.8×10^{10} cm^{-2}) dots began to form as shown in Fig. 2b, indicating initiation of the self-organized QD formation process. At GaInNAs thickness of 6 ml, dense dots with sheet density of ~6×10^{10} cm^{-2} can be seen from the AFM image in Fig. 2c. The dots have average height of ~5 nm and lateral diameter of ~33 nm with relatively homogenous distribution. Further increase in thickness to 7 ml and beyond results in coalescence of the dots leading to significant surface roughening (RMS surface roughness > 2 nm). Figure 2d and e show the cross-sectional TEM images of 4.5 ml-thick $Ga_{0.6}In_{0.4}N_{0.01}As_{0.99}$ QDs and 5 ml-thick $Ga_{0.5}In_{0.5}N_{0.01}As_{0.99}$ QDs multilayer samples, respectively. The images show coherent dot profile with aspect ratio of ~0.1. This is in good agreement with the AFM measurements, in terms of dot size.

The critical thickness is an important parameter governing the self-organized growth kinetics. Using in situ RHEED observation, the transition time to change from 2D to 3D growth mode can be used to estimate the value of critical thickness. Critical thickness values of 3 ml and 2.5 ml have been reported for gas-source molecular beam epitaxy (GSMBE)-grown $Ga_{0.3}In_{0.7}N_{0.04}As_{0.96}$ and $InN_{0.02}As_{0.98}$ QDs, respectively [23]. For metalorganic vapor phase epitaxy (MOVPE)-grown

$Ga_{0.4}In_{0.6}(N)As$ QDs [35], critical thickness value of 3 ml has been reported. Figure 3 shows the variation in critical thickness for SSMBE-grown GaInNAs QDs of different In compositions (30–100%) as function of N composition (0–1.5%). It can be seen that the GaInNAs critical thickness decreased drastically from 10–15 nm to < 1 nm as the In composition is increased from 30% to 100%. This is because the GaInNAs-to-GaAs layer strain is mainly determined by the In composition at low N content. For GaInNAs samples of the same In composition, the dependence of critical thickness on N composition show obvious fluctuations with respect to theoretical expectation. In general, the critical thickness required for spontaneous SK island formation is inversely proportional to square of the misfit of the strained layer [39, 40]. This is represented by dotted lines in the figure. It can be seen that the experimental data is quite different from theoretical expectations. A possible reason for such deviation is the non-uniformity in composition or strain in the GaInNAs layer, which will be discussed further in the following section. Furthermore, it was found that the fluctuation of critical thickness is less significant in GaInNAs at higher In composition. This could suggest that the non-uniformity in composition or strain caused by N incorporation plays a relatively weaker role compared to the strain effects at high In composition.

Depending on growth conditions [23, 34, 35], GaInNAs QD density can reach levels as high as 10^{10}–10^{11} cm^{-2} with average dot height in the range of 2–16 nm and dot lateral diameter in the range of 20–45 nm. Thickness and material composition are basic parameters, which impact the QD structural properties. Figure 4 shows the dot density and average dot height of GaInNAs QDs grown by SSMBE, as function of thickness at different In composition [41]. As expected, increasing the surface coverage results in greater dot density and dot height. Moreover, for GaInNAs of high In composition, high-density dots can be formed at relatively lower surface coverage. Besides smaller critical thickness in GaInNAs at high In composition, another possible reason for this observation is the strong local strain caused by N incorporation. This enhances the formation of strained dots, especially in GaInNAs of high In composition [42]. The incorporation of N has a complicated influence on the QD size and density. Some experiments have suggested that low N incorporation results in smaller GaInNAs QD size and much higher dot density compared to InGaAs QDs grown under identical conditions [23, 31, 35]. However, this behavioral trend may not be true at N composition $> 1\%$, where there are reports of dot coalescence resulting in low-density, large sized incoherent GaInNAs dots [23, 31, 33]. On the contrary, some experiments on InNAs QDs [43] and GaInNAs QDs [44] grown by GSMBE have shown that introduction of N induces a reduction in dot density and increase in dot sizes. As far as QD size uniformity is concerned, experiments have shown that the growth

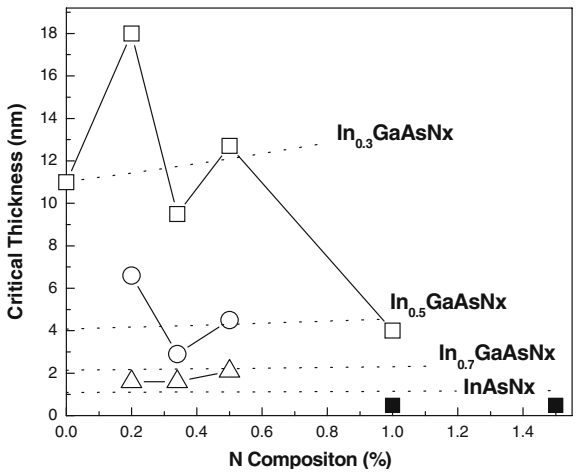

Fig. 3 The variation in critical thickness for SSMBE-grown GaInNAs QDs with different In and N compositions, estimated from RHEED observations

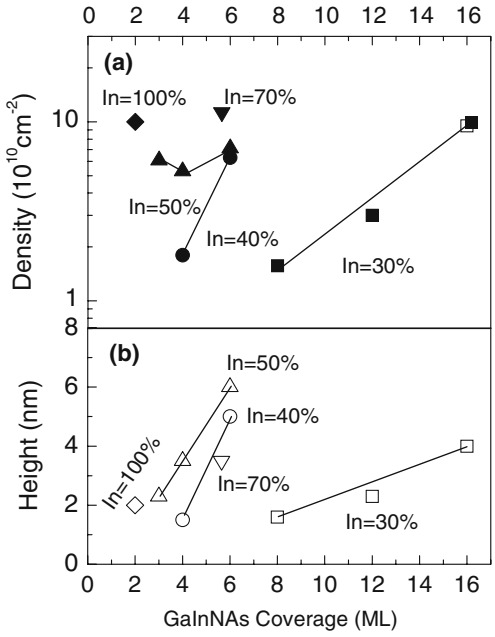

Fig. 4 (**a**) Dot density, and (**b**) Average dot height measured by AFM as function of GaInNAs surface coverage. The In composition was varied from 30% to 100%. The N composition was 0.4% for the sample with 70% In and ~1% for all other samples. The lines serve as guide for the eye

kinetics governing GaInNAs and InGaAs QD formation are significantly different [23, 43].

In terms of the optical properties of GaInNAs QDs, the principal target is to extend the emission wavelength. As a rough estimate, 1% of N incorporation will cause ~200 meV in energy shift assuming bowing coefficient of 20 eV. The effectiveness of N incorporation on wavelength extension had been experimentally confirmed. Figure 5 shows the PL spectrum from a sample with one $Ga_{0.7}In_{0.3}As$ QD layer and one $Ga_{0.7}In_{0.3}N_{0.006}As$ QD layer grown by SSMBE under identical conditions. Separate PL peaks were detected from the two different QD layers. It can be seen that the PL peak was shifted by 45 nm (or ~56 meV) following the introduction of ~0.6% N into the $Ga_{0.7}In_{0.3}N_{0.006}As$ QD layer. This clearly shows the effect of N incorporation on the emission property of GaInNAs QDs. Similar results on red shift in energy from ~1.2 eV to 1.08 eV was reported for SSMBE-grown $Ga_{0.7}In_{0.3}AsN$ QDs following increase in N content from 0% to ~1% [24]. Ballet et al. [43] have reported RT emission at ~1.28 μm (~0.97 eV) from InAsN/GaAs QDs with 0.8% N. This represents a 80 meV energy shift compared to emission at 1.18 μm (~1.05 eV) from InAs/GaAs QDs grown by GSMBE. Furthermore, it was reported that increasing the N content to 2.1% has failed to extend the wavelength further in this experiment. This could be due to non-uniform N concentration in the InAsN QDs and the presence of defects at high N levels. Sopanen et al. [23] have reported PL emission at 1.3 μm and 1.52 μm from 4 ml-$Ga_{0.3}In_{0.7}N_{0.02}As_{0.96}$ QDs and 5.5 ml-$Ga_{0.3}In_{0.7}N_{0.04}As_{0.96}$ grown by GSMBE. Although the PL spectrum was relatively weak and broad, the results paved the way for long wavelength tuning using such QD layers.

Apart from N concentration, the QD size, which depends on the layer thickness, also affects the emission wavelength due to its effect on the quantum confinement. Figure 6(a–c) shows the 5 K PL spectra of SSMBE-grown $Ga_{0.5}In_{0.5}N_{0.01}As_{0.99}$ QDs of different layer thickness from 4 ml to 7.5 ml. No PL signal from the wetting layer was detected, and each spectrum shows a strong PL peak originating from the QD layer. Generally, the PL peaks are relatively broad due to fluctuation in QD sizes, and the full-width at half maximum (FWHM) ranges from 60 nm to 90 nm. As the thickness of the dot layer is increased from 4 ml to 7.5 ml, the PL peak red-shifted from 900 nm to 1,100 nm. The shift to longer wavelength is attributed to increase in dot sizes. However, this method has its limitations as the thickness continues to increase, since significant structural degradation will occur as the strain accumulates following increase in thickness. It can be seen that the 5 ml-thick $Ga_{0.5}In_{0.5}N_{0.01}As_{0.99}$ QD sample exhibits the strongest PL intensity, due to its higher dot density compared to the 4 ml-thick sample. At 7.5 ml, the PL intensity dropped rather significantly, suggesting the formation of strain-induced defects caused by high surface coverage. Similar observation is also reported for GaInNAs QDs grown by GSMBE [45].

In the well-studied InGaAs/GaAs QD system, modifying the dot structures by combining layers with different composition has proven to be effective for controlling the physical properties of self-assembled

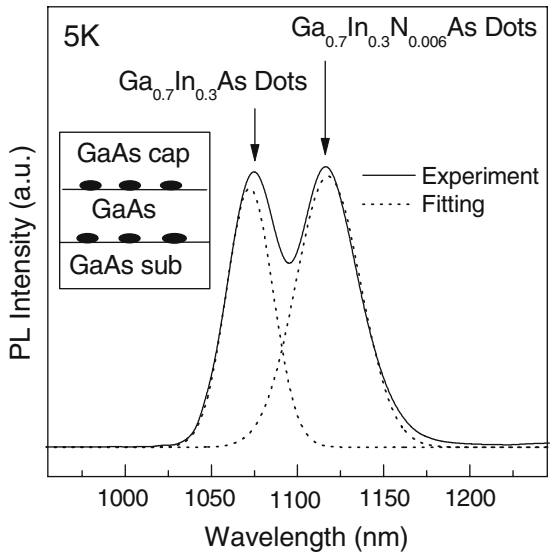

Fig. 5 PL spectra from SSMBE-grown sample with one $Ga_{0.7}In_{0.3}As$ dot layer and one $Ga_{0.7}In_{0.3}N_{0.006}As$ dot layer

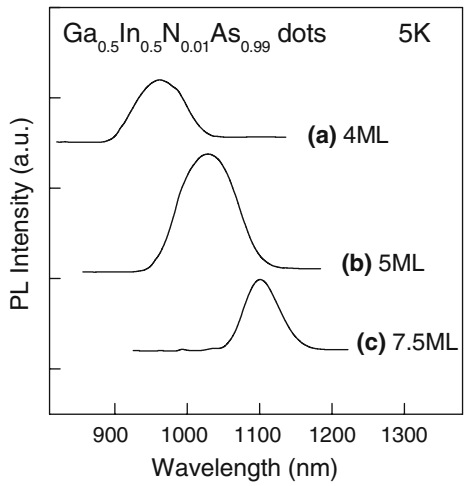

Fig. 6 5 K PL spectra of: (**a**) 4ml-thick, (**b**) 5 ml-thick, (**c**) 7.5 ml-thick $Ga_{0.5}In_{0.5}N_{0.01}As_{0.99}$ QDs

QDs [46, 47]. Generally, this method usually involves introducing an intermediate layer before and/or after the QD layer. Such layers are also known as strain reducing layer (SRL) or strain compensating layer (SCL). The intermediate layer has different lattice constant or energy gap compared to the dot layer and barrier layer. Its presence will modify the strain field or quantum confinement conditions of the dot layer. A properly designed intermediate layer can improve the dot size uniformity and extend the emission wavelength. There have been some studies on GaInNAs QDs, where GaAsN intermediate layers were inserted between the GaAs barrier and GaInNAs QD layer for extending the emission wavelength of the GaInNAs QDs. Nishikawa et al. have reported a study which compared GSMBE-grown $GaInN_{0.02}As$/GaAs QD samples with: (a) no intermediate layer, (b) $GaAsN_{0.02}$ intermediate layer after the dots, and (c) $GaAsN_{0.02}$ intermediate layers before and after the dots [45]. Due to lower confinement provided by the GaAsN intermediate layer compared to GaAs, the QD emission wavelength shifts to 1.38 μm at 10 K and 1.48 μm at RT with GaAsN intermediate layer. However, this is accompanied by decrease in the PL intensity. We have investigated the effect of GaAsN intermediate layer on the surface morphology of SSMBE-grown GaInNAs QDs. Figure 7 shows the AFM images taken on uncapped 5 ml-thick $Ga_{0.5}In_{0.5}N_{0.01}As_{0.99}$ QD samples with GaAsN intermediate layer of different thickness (0, 5, and 10 nm). Figure 7a shows GaInNAs QDs grown on GaAs have average diameter d ~33 nm, height h ~5 nm, and surface density $\rho \sim 8.6 \times 10^{10}/cm^2$. As seen in Fig. 7b, GaInNAs dots grown on 5 nm-thick GaAsN have similar dot sizes and density (d ~ 30 nm, h ~ 4.8 nm, $\rho \sim 1.1 \times 10^{11}/cm^2$) and appeared to have better uniformity. However, increasing the GaAsN thickness to 10 nm or more resulted in significant increase in surface roughness, as shown in Fig. 7c. In this case, the GaInNAs dots appeared rather irregular with poor uniformity. The change in QD uniformity associated with the GaAsN intermediate layer before the dot layer is possibly due to the introduction of composition/thickness modulation by the intermediate layer. The GaAsN intermediate layer may form slight undulations and the resulting surface strain will assume certain periodic characteristic, where preferential GaInNAs QD nucleation on some periodic sites may occur. Furthermore, a GaAsN intermediate layer inserted above the QD layer can reduce the strain between the QD layer and GaAs cap layer. This can lower the formation of interface dislocations. However, an overly thick GaAsN intermediate layer should be avoided to minimize dislocation formation due to strong surface undulations caused by high total strain energy.

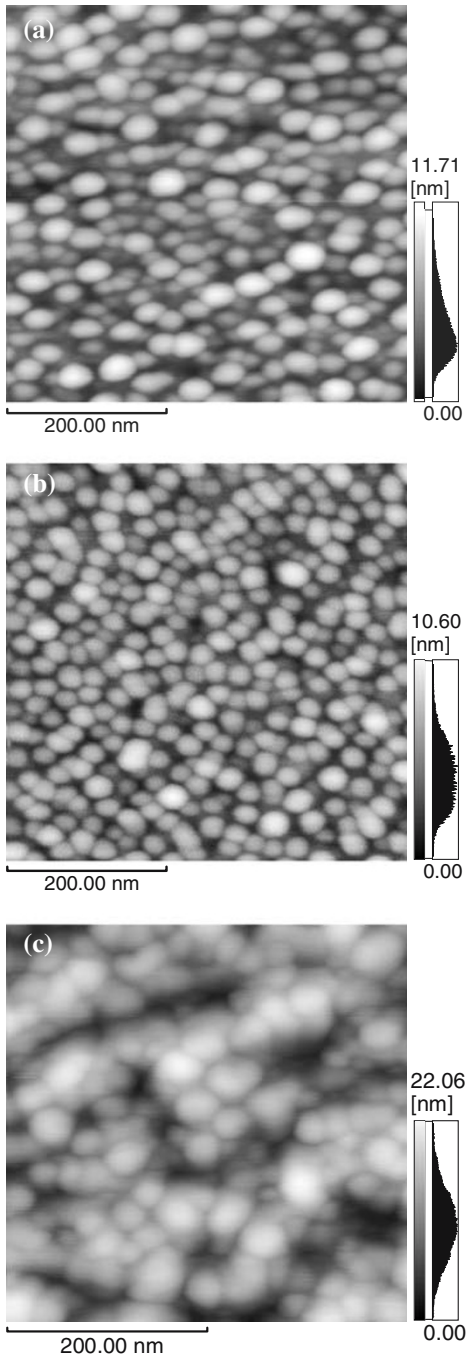

Fig. 7 Comparison of AFM morphology of uncapped $Ga_{0.5}In_{0.5}N_{0.01}As_{0.99}$ QD samples with different $GaAsN_{0.01}$ intermediate layer thickness of (**a**) 0 nm, (**b**) 5 nm, and (**c**) 10 nm. The scanned area is 0.5 μm × 0.5μm

Based on the above mentioned results on structural and optical properties of GaInNAs QDs, self-assembled $Ga_{0.7}In_{0.3}N_{0.01}As_{0.99}/GaAsN_{0.01}$ single layer QD laser structure has been grown. The growth details

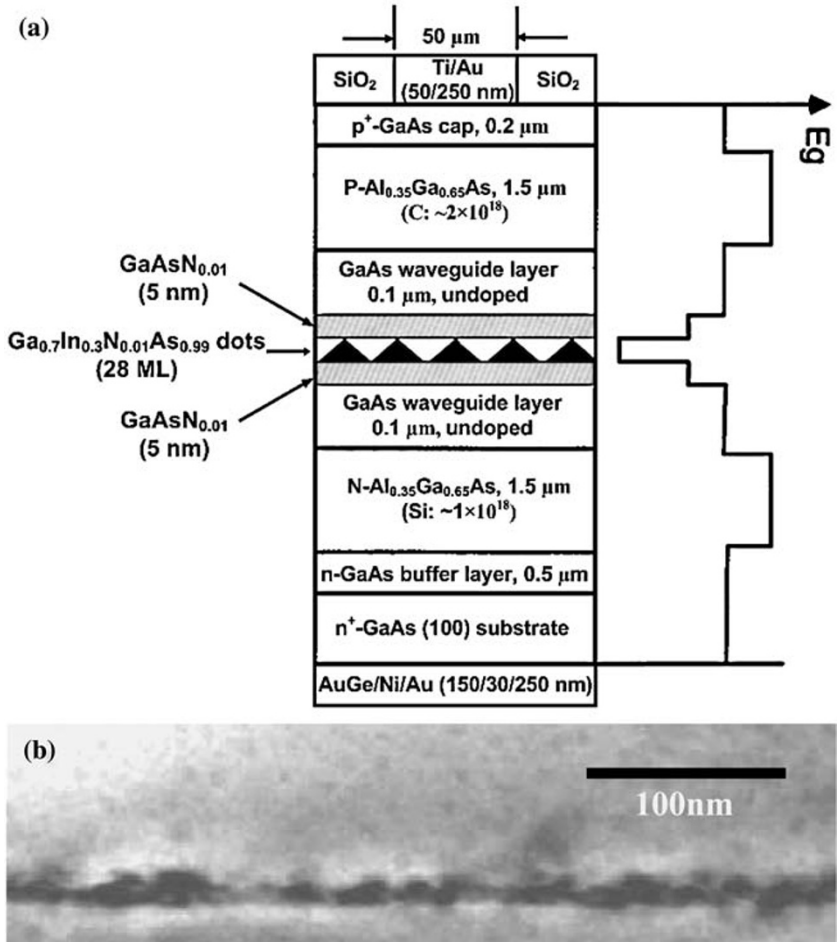

Fig. 8 Schematic cross-section, band diagram and layer structure of the GaInNAs/GaAsN QD laser (**a**) (not to scale) and a cross-sectional TEM image of the GaInNAs QD active region (**b**)

have been included in Section 2. Figure 8a shows the schematic cross-section, layer structure and band diagram of the fabricated $Ga_{0.7}In_{0.3}N_{0.01}As_{0.99}/GaAsN_{0.01}$ single layer QD edge emitting laser (not to scale). Figure 8(b) shows the TEM image of the GaInNAs QD active region.

Figure 9 shows the typical RT, CW $P - I$ characteristics of a p-side down bonded GaInNAs QD laser with dimension of $50 \times 2{,}000$ μm^2. The laser has threshold current (I_{th}) of 2.2 A, corresponding to J_{th} of ~2.2 kA/cm^2, which was determined by the measured I_{th} divided by contact area ($w \times L$). Light output power of 16 mW/facet was achieved from this device. The inset of Fig. 9 shows the lasing spectrum of the same laser with peak wavelength centered at 1175.86 nm and mode width $\Delta\lambda$ of 0.037 nm. The laser emission spectra were measured in CW mode using a spectrometer with resolution of 0.025 nm, an InGaAs detector (cooled down to – 30 °C), and a data acquisition system.

Figure 10 shows the $P - I$ characteristics at 10 °C of the unbonded as-cleaved GaInNAs QD lasers with L of 500 μm and 1,700 μm, respectively, under pulsed operation. The lowest I_{th} around 375 mA was obtained from the GaInNAs QD laser (50×500 μm^2), corresponding to J_{th} of 1.5 kA/cm^2. There is an observed kink effect in the $P - I$ curve of the 500-μm-long laser,

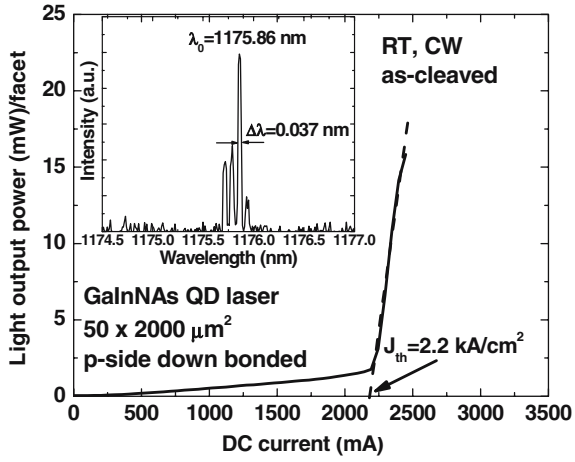

Fig. 9 RT, CW $P - I$ characteristics of a p-side down bonded GaInNAs QD laser, with dimension of $50 \times 2{,}000$ μm^2. The inset shows the corresponding RT, CW lasing spectrum

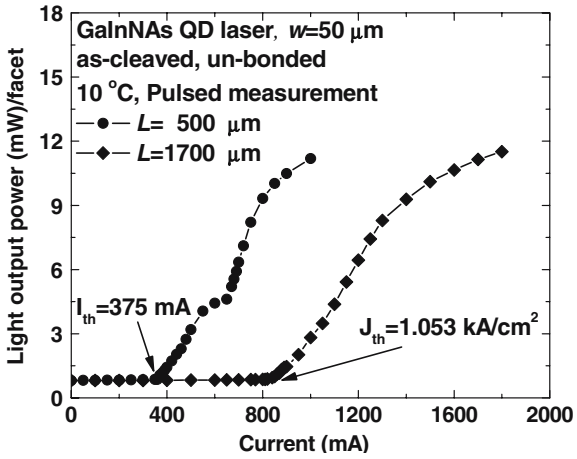

Fig. 10 $P - I$ characteristics of GaInNAs QD lasers with cavity length (L) of 500 μm and 1,700 μm, respectively. The as-cleaved lasers were tested under pulsed operation without bonding at 10 °C

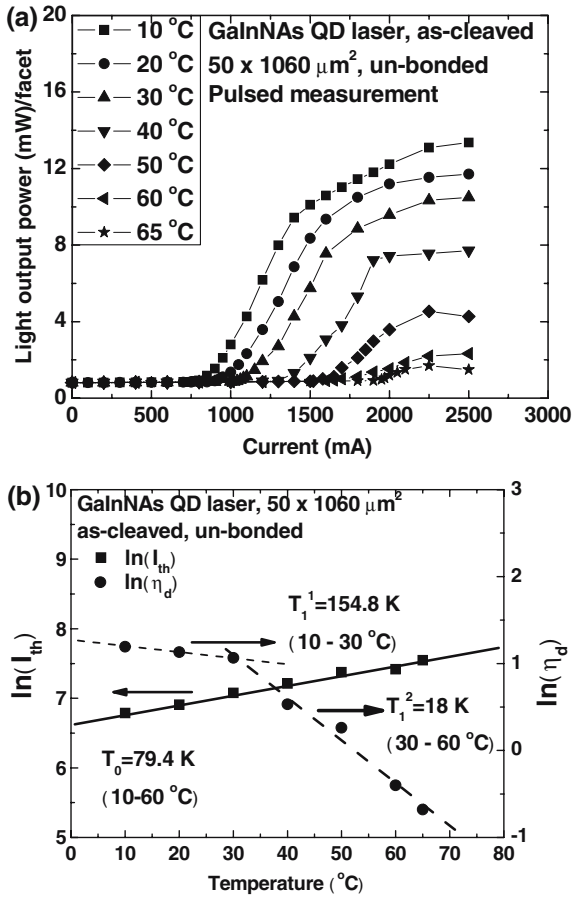

Fig. 11 (**a**) Temperature-dependent (10–65 °C) $P - I$ characteristics of GaInNAs QD lasers with dimension of 50 × 1,060 μm^2. The as-cleaved laser was tested under pulsed operation without bonding. (**b**) Plot of ln(I_{th}) versus T (left axis) and ln(η_d) versus T (right axis) for GaInNAs QD laser. T_0 was estimated to be 79.4 K in the temperature range of 10–60 °C. T_1 was estimated to be 154.8 K (10–30 °C) and 18 K (30–60 °C), respectively

which is mode hopping between the longitudinal cavity modes, typical in the Fabry-Perot semiconductor laser diodes[48]. The GaInNAs QD laser, with dimension of 50 × 1,700 μm^2, has the lowest measured J_{th} of 1.053 kA/cm^2 among all the tested devices. This J_{th} is much lower than that of the longer devices (L = 2,000 μm) under CW operation in Fig. 9, which is 2.2 kA/cm^2. This suggests that the device heating in the CW mode is high in our GaInNAs QD lasers.

Figure 11a shows the temperature-dependent (10–65 °C) $P - I$ characteristics of an unbonded GaInNAs QD lasers with dimension of 50 × 1,060 μm^{2}under pulsed measurement. This device successfully lased up to 65 °C. To the best of our knowledge, this is the highest temperature GaInNAs QD laser operation ever reported. Figure 11b shows the plot of ln(I_{th}) versus temperature (T) (left axis) and logarithm of external quantum efficiency, ln(η_d) versus T (right axis). The dots denote the experimental data and the lines are used for eye guidance. By fitting the experimental data using Eqs. (1) and (2), T_0 was extracted to be 79.4 K in the temperature range of 10–60 °C; T_1 (characteristic temperature of η_d) was estimated to be 154.8 K (10–30 °C) and 18 K (30–60 °C), respectively.

$$I_{\text{th}} = I_0 \exp\left(\frac{T}{T_0}\right) \tag{1}$$

$$\eta_d = \eta_0 \exp\left(\frac{-T}{T_1}\right) \tag{2}$$

where η_d of the GaInNAs QD laser was determined by $\eta_d = 2 \times \frac{\Delta P}{\Delta I} \times \frac{q\lambda}{hc}$, and $\Delta P/\Delta I$ was obtained from the measured $P - I$ characteristics. h Is the Planck's constant, q the electronic charge, c the speed of light in vacuum, and λ the emission wavelength of the GaInNAs QD laser.

The η_d value of this work is only 3.3 % (10 °C) and 0.5% (65 °C). Huffaker et al. have also reported low η_d ~3% from InGaAs QD laser (40 μm × 5.1 mm) at 295 K [49]. They attributed the low η_d to the long cavity length. In our case, the low efficiency suggests the possible presence of non-radiative recombination centers in the $Ga_{0.7}In_{0.3}N_{0.01}As_{0.99}/GaAsN_{0.01}$ QD laser structure, most likely in the GaInNAs QD layer, or GaAsN wetting layer due to defects caused by nitrogen incorporation, or at the AlGaAs/GaAs hetero-interfaces [38, 50].

Temperature-dependent $P - I$ characteristics were also measured from an unbonded as-cleaved GaInNAs QD laser with longer L of 1,700 μm. Figure 12 shows the temperature-dependent (10–50 °C) $P - I$ characteristics of a GaInNAs QD laser (50 × 1,700 μm^2)

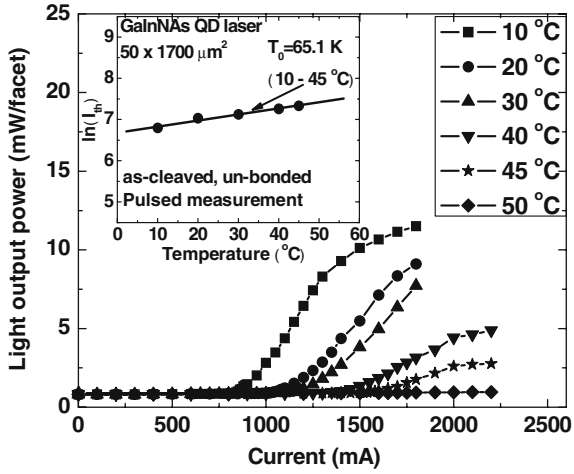

Fig. 12 Temperature-dependent (10–50 °C) $P - I$ characteristics of GaInNAs QD lasers with dimension of $50 \times 1{,}700$ μm^2. The as-cleaved laser was tested under pulsed operation without bonding. The inset shows $\ln(I_{th})$ as function of temperature. T_0 was estimated to be 65.1 K in the temperature range of 10–45 °C

under pulsed measurement. The laser could only operate up to 45 °C. As shown in the inset of Fig. 12, the plot of $\ln(I_{th})$ versus T exhibits linear behavior in the range of 10–45 °C, and yielded T_0 of 65.1 K using Eq. (1). This value is much lower than that of the GaInNAs QD laser with L of 1,060 μm, which is 79.4 K. Mukai et al. demonstrated higher T_0 from InGaAs QD laser with longer cavity length. They reported that carrier overflow into the upper sublevels is reduced in long-cavity lasers since the threshold gain becomes smaller due to decrease in cavity loss [51]. This is consistent with the recently derived physical parameter-dependent semiconductor laser characteristics [15]. By assuming J_{th}, J_{tr}, and internal optical loss (α_i) to increase exponentially with T, while η_d, material gain (g_0), current injection efficiency (η_{inj}) to decrease exponentially with T, Eq. (3) could be used to express T_0 as function of the physical parameters of the semiconductor laser in Ref. [15] and references therein.

$$\frac{1}{T_0(L)} = \frac{1}{T_{tr}} + \frac{1}{T_{\eta_{inj}}} + \frac{\Gamma \cdot g_{th}(= \alpha_i + \frac{1}{L}\ln\frac{1}{R})}{\Gamma \cdot g_0} \cdot \frac{1}{T_{g_0}} + \frac{\alpha_i}{\Gamma \cdot g_0} \cdot \frac{1}{T_{\alpha_i}} \quad (3)$$

where T_{tr}, $T_{\eta_{inj}}$, T_{g_0}, and T_{α_i} are the characteristic temperatures of J_{tr}, η_{inj}, g_0, and α_i, respectively.

From the above equation, it can also be seen that for a semiconductor laser, when L is shorter, T_0 is lower due to the higher threshold gain ($\Gamma \cdot g_{th} = \alpha_i + \frac{1}{L}\ln\frac{1}{R}$), and *vice versa*. However, Shchekin et al. observed lower T_0 from longer InAs QD lasers, which was attributed to higher device heating in longer devices.[52] Furthermore, Gao et al. also reported that J_{th} in their GaInNAs QD lasers increased with longer cavity length, instead of decrease, which is normally observed in semiconductor laser diodes [38]. This was attributed to the overwhelming influence of non-radiative recombination in the GaInNAs QD structure caused mainly by non-uniformity of the QDs, which is expected to be higher in longer devices. Since our measurements were carried out under pulsed operation, we assume device heating can be neglected. Therefore, based on the above discussions, it is possible that the observed T_0 decrease with increase in cavity length in our GaInNAs QD laser be due to non-uniformity of the QD layer.

Despite the above possible effects, compared with the reported GaInNAs QD laser results [31, 38], our GaInNAs QD lasers have shown significant improvement in performance with high temperature operation up to 65 °C, high T_0 of 79.4 K, and low J_{th} of 1.05 kA/cm^2. Though these results are still inferior compared to their GaInNAs QW counterparts [3–19] and In(Ga)As QD lasers [49–53], however, the results in this work indicate that GaInNAs QDs have potential for long-wavelength semiconductor laser application. Further improvement and optimization in the GaInNAs QD material growth are on-going for better crystal quality, higher GaInNAs QD densities and longer wavelength. In the present work, single GaInNAs QD layer has been adopted; while in the future, the limited modal gain in QD lasers can be partly alleviated by stacking several high quality QD layers [51, 53]. Furthermore, our recent work has shown that by suppressing the lateral current spreading in broad area lasers, the RWG laser performance can be greatly improved [17]. Therefore, further improvement of the GaInNAs QD laser would also include optimization of the waveguide structure in the fabrication. With the above optimization, it is expected that the performance of the GaInNAs QD laser could be further improved.

Summary and future challenges in dilute nitride Qds

In summary, it can be stated that studies on dilute nitride QDs are still in the initial stages. Epitaxial growth characteristics, structural and optical properties of GaInNAs QDs are presently under active investigations by many groups. Although GaInNAs QD lasers operating CW at room temperature at ~1.2 μm have been demonstrated, there is still much to be done to further extend the wavelength, reduce the threshold current density and improve the operating lifetime.

In terms of wavelength and laser performance, present day data from GaInNAs QDs are not as good as those from InGaAs QDs and GaInNAs QW devices. Therefore, there is a need for greater research efforts to improve the performance of GaInNAs QD devices. Compared to InGaAs/GaAs QDs, GaInNAs/GaAs QDs faces a key challenge of minimizing the formation of N-induced defects, as more N incorporation is needed to extend the emission wavelength to higher values. Interactions within the quaternary compound itself will not make the growth optimization process any easier to achieve good QD size uniformity and density. Compared to GaInNAs/GaAs QWs, GaInNAs/GaAs QDs will face key challenges to seek solutions to suppress strain-related defects and improve QD size uniformity. Breakthroughs in growth optimization and structure optimization are needed to realize the potential of GaInNAs/GaAs QDs for application in long wavelength lasers.

Acknowledgments The authors are grateful to A*STAR for providing financial support in this research through the ONFIG-II program. TEM support from Tung Chih-Hang, Du An Yan and Doan My The of the Institute of Microelectronics, Singapore, as well as discussions with Prof. B.X. Bo of Changchun University of Science and Technology, Dr Mei Ting, Nie Dong, and Dr Tong Cunzhu of the School of Electrical and Electronic Engineering, Nanyang Technological University, is acknowledged.

References

1. N.K. Dutta, R.J. Nelson, Appl. Phys. Lett. **38**, 407 (1981)
2. E. Yablonovitch, O.E. Kane, J. Lightwave Technol. **4**, 504 (1986)
3. M. Kondow, K. Uomi, A. Niwa, T. Kitatani, S. Watahiki, Y.Yazawa, Jpn. J. Appl. Phys. **35**, 1273 (1996)
4. M. Kondow, T. Kitatani, S. Nakatsuka, M.C. Larson, K. Nakahara, Y. Yazawa, M. Okai, K. Uomi, IEEE J. Sel. Top. Quantum Electron. **3**, 719 (1997)
5. J.S. Harris Jr., IEEE J. Sel. Top. Quantum Electron. **6**, 1145 (2000)
6. J.S. Harris Jr., Semicond. Sci. Technol. **17**, 880 (2002)
7. W. Ha, V. Gambin, M. Wistey, S. Bank, S. Kim, J.S. Harris Jr., IEEE Photon. Technol. Lett. **14**, 591 (2002)
8. R. Fehse, S. Tomic, A.R. Adams, S.J. Sweeney, E.P. O'Reilly, A. Andreev, H. Riechert, IEEE J. Sel. Top. Quantum Electron. **8**, 801 (2002)
9. A.R. Kovsh, J.S. Wang, R.S. Hsiao, L.P. Chen, D.A. Livshits, G. Lin, V.M. Ustinov, J.Y. Chi, Electron. Lett. **39**, 1276 (2003)
10. D. Gollub, S. Moses, A. Forchel, IEEE J. Quantum Electron. **40**, 337 (2004)
11. S.M. Wang, Y.Q. Wei, X.D. Wang, Q.X. Zhao, M. Sadeghi, A. Larsson, J. Cryst. Growth, **278**, 734 (2005)
12. A. Hierro, J.M. Ulloa, E. Calleja, B. Damilano, J. Barjon, J.-Y. Duboz, and J. Massies, IEEE Photon. Technol. Lett. **17**, 1142 (2005)
13. B. Dagens, A. Martinez, D. Make, O.L. Gouezigou, J.G. Provost, V. Sallet, K. Merghem, J.C. Harmand, A. Ramdane, B. Thedrez, IEEE Photon. Technol. Lett. **17**, 971 (2005)
14. N. Tansu, J.-Y. Yeh, L.J. Mawst, IEEE J. Select. Top. Quantum Electron. **9**, 1220 (2003)
15. J.Y. Yeh, N. Tansu, L.J. Mawst, IEEE Photon. Technol. Lett. **16**, 741 (2004)
16. C.Y. Liu, S.F. Yoon, S.Z. Wang, W.J. Fan, Y. Qu, S. Yuan, IEEE Photon. Technol. Lett. **16**, 2409 (2004)
17. C.Y. Liu, Y. Qu, S. Yuan, S.F. Yoon, Appl. Phys. Lett. **85**, 4594 (2004)
18. N. Tansu, L.J. Mawst, J. Appl. Phys. **97**, 054502 (2005)
19. M. Yamada, T. Anan, H. Hatakeyama, K. Tokutome, N. Suzuki, T. Nakamura, and K. Nishi, IEEE Photon. Technol. Lett. **17**, 950 (2005)
20. Y. Arakawa, H. Sakaki, Appl. Phys. Lett. **40**, 939 (1982)
21. M. Asada, Y. Miyamato, Y. Suematsu, IEEE J. Quantum Electron. **22**, 1915 (1986)
22. T. Miyamoto, S. Makino, Y. Ikenaga, M. Ohta, F. Koyama, IEE Proce. Optoelectr. **150**, 59 (2003)
23. M. Sopanen, H.P. Xin, C.W. Tu, Appl. Phys. Lett. **76**, 994 (2000)
24. B.V. Volovik, A.R. Kovsh, W. Passenberg, H. Kuenzel, N. Grote, N.A. Cherkashin, Y.G Musikhin, N.N. ledentsov, D. Bimberg, V.M. Ustinov, Semicond. Sci. Technol. **16**, 186 (2001)
25. Z.Z. Sun, S.F. Yoon, K.C. Yew, W.K. Loke, S.Z. Wang, T.K. Ng, J. Gryst. Growth **242**, 109 (2002)
26. A. Nishikawa, Y.G. Hong, C.W. Tu, Phys. Stat. Solidi B **240**, 310 (2003)
27. K.C. Yew, S.F. Yoon, Z.Z. Sun, S.Z. Wang, J. Cryst. Growth **247**, 279 (2003)
28. Z.Z. Sun, S.F. Yoon, K.C. Yew, J. Cryst. Growth **259**, 40 (2003)
29. K.C. Yew, S.F. Yoon, Z.Z. Sun, J. Vac. Sci. Technol. B **21**, 2428 (2003)
30. Z.Z. Sun, S.F. Yoon, K.C. Yew, B.X. Bo, A.Y. Du, C.H. Tung, Appl. Phys. Lett. **85**, 1469 (2004)
31. S. Makino, T. Miyamoto, T. Kageyama, N. Nishiyama, F. Koyama, K. Iga, J. Cryst. Growth **221**, 561 (2000)
32. T. Miyamoto, T. Kageyama, S. Makino, Y. Ikenaga, F. Koyama, K. Iga, Proce. SPIE Int. Soc. Optical Eng. **4283**, 24 (2001)
33. S. Makino, T. Miyamoto, T. Kageyama, Y. Ikenaga, F. Koyama, K. Iga, Jpn. J. Appl. Phys. **41**, 953 (2002)
34. S. Makino, T. Miyamoto, M. Ohta, T. Kageyama, Y. Ikenaga, F. Koyama, K. Iga, J. Cryst. Growth **251**, 372 (2003)
35. T. Hakkarainen, J. Toivonen, M. Sopanen, H. Lipsanen, Appl. Phys. Lett. **79**, 3932, (2001)
36. V.M. Daniltsev, M.N. Drozdov, Yu. N. Drozdov, D.M. Gaponova, O.I. Khrykin, A.V. Murel, V.I. Shashkin, N.V. Vostrokov, J. Cryst. Growth **248**, 343 (2003)
37. Y.D. Jang, J.S. Yim, U.H. Lee, D. Lee, J.W. Jang, K.H. Park, W.G. Jeong, J.H. Lee, D.K. Oh, Phys. E **17**, 127 (2003)
38. Q. Gao, M. Buda, H.H. Tan, C. Jagadish, Electrochem. Solid-State Lett. **8**, G57 (2005)
39. B.W. Wessels, J. Vac. Sci. Technol. B **15**, 1056 (1997)
40. P.M. Petroff, S.P. DenBaars, Superlattices Microst. **15**, 15 (1994)
41. Z.Z. Sun, S.F. Yoon, K.C. Yew, B.X. Bo, Mat. Res. Soc. Symp. Proc. **794** T3.31.1, Boston (2003)
42. H.P. Xin, K.L. Kavanagh, Z.Q. Zhu, C.W. Tu, Appl. Phys. Lett. **74**, 2337 (1999)
43. P. Ballet, P.Gilet, L. Grenouillet, P. Duvaut, G. Feuillet, A. Million, Mat. Res. Soc. Symp. Proc. **642**, J3.33 (2001)
44. A. Nishikawa, Y.G. Hong, C.W. Tu, Physica Status Solidi B **240**, 310 (2003)
45. A. Nishikawa, Y.G. Hong, C.W. Tu, 2003 International Conference Indium Phosphide and Related Materials. Conference Proceedings, ThB 1. **7**, 359 (2003)

46. K. Nishi, H. Saito, S. Sugou, J.S. Lee, Appl. Phys. Lett. **74**, 1112 (1999)
47. J. Ahopelto, H. Lipsanen, M. Sopanen, T. Koljonen, H.E.-M. Niemi, Appl. Phys. Lett. **65**, 1662 (1994)
48. J.K. White, J.V. Moloney, IEEE J. Select. Top. Quantum Electron. **9**, 816 (2003)
49. D.L. Huffaker, G. Park, Z. Zou, O.B. Shchekin, D.G. Deppe, Appl. Phys. Lett. **73**, 2564 (1998)
50. G. Park, D.L. Huffaker, Z. Zou, O.B. Shckekin, D.G. Deppe, IEEE Photon. Technol. Lett. **11**, 301 (1999)
51. K. Mukai, Y. Nakata, K. Otsubo, M. Sugawara, N. Yokoyama, H. Ishikawa, IEEE J. Quantum Electron. **36**, 472 (2000)
52. O.B. Shchekin, D.G. Deppe, IEEE Photon. Technol. Lett. **14**, 1231 (2002)
53. A.R. Kovsh, N.A. Maleev, A.E. Zhukov, S.S. Mikhrin, A.R. Vasilev, Y. M. Shemyakov, M.V. Maximov, D.A. Livshits, V. Ustinov, Zh. I. Alferov, N. N. Ledentsov, D. Bimberg, Electron. Lett. **38**, 1104 (2002)